Heart

In Vivo Alpha-V Beta-3 Integrin Expression in Human Aortic Atherosclerosis

Journal:	*Heart*
Manuscript ID	heartjnl-2019-315103.R1
Article Type:	Original research article
Date Submitted by the Author:	13-May-2019
Complete List of Authors:	Jenkins, William; University of Edinburgh, Centre for Cardiovascular Science Vesey, Alex; University of Edinburgh, Centre for Cardiovascular Science Vickers, Anna; University of Edinburgh, Centre for Cardiovascular Science Neale, Anoushka; University of Edinburgh, Centre for Cardiovascular Science Moles, Catriona; University of Edinburgh, Centre for Cardiovascular Science Connell, Martin; University of Edinburgh Joshi, Nikhil; University of Edinburgh, Centre for Cardiovascular Science Lucatelli, Christophe; University of Edinburgh, Clinical Research Imaging Centre Fletcher, Alison; University of Edinburgh, Clinical Research Imaging Centre Spratt, James; University of Edinburgh, Department of Cardiovascular Sciences Mirsadraee, Saeed; University of Edinburgh, Clinical Research Imaging Centre van Beek, Edwin; University of Edinburgh, Clinical Research Imaging Centre Rudd, James; University of Cambridge, Division of Cardiovascular Medicine Newby, David; University of Edinburgh, Centre for Cardiovascular Sciences Dweck, Marc; University of Edinburgh, Centre for Cardiovascular Sciences
Keywords:	Positron emission tomographic (PET) imaging < Cardiac imaging and diagnostics < CARDIAC PROCEDURES AND THERAPY, Cardiac computer tomographic (CT) imaging < Cardiac imaging and diagnostics < CARDIAC PROCEDURES AND THERAPY, Aortic and arterial disease < DISEASES
Abstract:	Objectives Intra-plaque angiogenesis and inflammation are key promoters of atherosclerosis and are mediated by the $\alpha v\beta 3$ integrin pathway. We investigated the applicability of the $\alpha v\beta 3$-integrin receptor-selective positron emission tomography (PET) radiotracer 18F-fluciclatide in

assessing human aortic atherosclerosis.

Methods
Vascular 18F-fluciclatide binding was evaluated using ex vivo analysis of carotid endarterectomy samples with autoradiography and immunohistochemistry, and in vivo kinetic modeling following radiotracer administration. Forty-six subjects with a spectrum of atherosclerotic disease categorized as stable (n=27) or unstable (n=19; recent myocardial infarction) underwent PET and computed tomography (CT) imaging of the thorax after administration of 226±13 MBq 18F-fluciclatide. Thoracic aortic 18F-fluciclatide uptake was quantified on fused PET-CT images and corrected for blood-pool activity using the maximum tissue-to-background ratio (TBRmax). Aortic atherosclerotic burden was quantified by CT wall thickness, plaque volume and calcium scoring.

Results
18F-Fluciclatide uptake co-localised with regions of increased αvβ3 integrin expression, and markers of inflammation and angiogenesis. 18F-Fluciclatide vascular uptake was confirmed in vivo using kinetic modeling, and on static imaging correlated with measures of aortic atherosclerotic burden: wall thickness (r=0.57, p=0.001), total plaque volume (r=0.56, p=0.001) and aortic CT calcium score (r=0.37, p=0.01). Patients with recent myocardial infarction had greater aortic 18F-fluciclatide uptake than those with stable disease (TBRmax 1.33 vs 1.21, p=0.01).

Conclusions
In vivo expression of αvβ3 integrin in human aortic atheroma is associated with plaque burden and is increased in patients with recent myocardial infarction. Quantification of αvβ3 integrin expression with 18F-fluciclatide PET has potential to assess plaque vulnerability and disease activity in atherosclerosis.

SCHOLARONE™
Manuscripts

In Vivo Alpha-V Beta-3 Integrin Expression in Human Aortic Atherosclerosis

Dr. William SA Jenkins, MD, PhD [1]

Dr. Alex T Vesey, MD [1]

Dr. Anna Vickers, MD [1]

Dr. Anoushka Neale, MD [1]

Dr. Catriona Moles, MD [1]

Mr Martin Connell, BSc [2]

Dr. Nik V Joshi, MD, PhD [1]

Dr. Christophe Lucatelli, PhD [2]

Dr. Alison M Fletcher, PhD [2]

Dr. James C Spratt, MD [1]

Dr. Saeed Mirsadraee, MD, PhD [2]

Professor Edwin JR Van Beek, MD, PhD [2]

Dr. James HF Rudd, MD, PhD [3]

Professor David E Newby, MD, PhD [1, 2]

Dr. Marc R Dweck, MD, PhD [1, 2]

[1] British Heart Foundation Centre for Cardiovascular Science, University of Edinburgh, Edinburgh

[2] Clinical Research Imaging Centre, University of Edinburgh, Edinburgh

[3] Division of Cardiovascular Medicine, University of Cambridge, Cambridge

Corresponding Author

Dr William SA Jenkins, Department of Cardiovascular Sciences, Room SU305, Chancellors Building, 49 Little France Crescent, University of Edinburgh, EH16 4SB.

Email; williamjenkins@nhs.net.

Tel: 0131 242 6515. Fax: 0131 242 6379

Word count; 3,056

1
2
3
4
5
6
7
8
9
10
11
12
13
14
15
16
17
18
19
20
21
22
23
24
25
26
27
28
29
30
31
32
33
34
35
36
37
38
39
40
41
42
43
44
45
46
47
48
49
50
51
52
53
54
55
56
57
58
59
60

Abstract

Objectives

Intra-plaque angiogenesis and inflammation are key promoters of atherosclerosis and are mediated by the $\alpha_v\beta_3$ integrin pathway. We investigated the applicability of the $\alpha_v\beta_3$-integrin receptor-selective positron emission tomography (PET) radiotracer 18F-fluciclatide in assessing human aortic atherosclerosis.

Methods

Vascular 18F-fluciclatide binding was evaluated using *ex vivo* analysis of carotid endarterectomy samples with autoradiography and immunohistochemistry, and *in vivo* kinetic modeling following radiotracer administration. Forty-six subjects with a spectrum of atherosclerotic disease categorized as stable (n=27) or unstable (n=19; recent myocardial infarction) underwent PET and computed tomography (CT) imaging of the thorax after administration of 226±13 MBq 18F-fluciclatide. Thoracic aortic 18F-fluciclatide uptake was quantified on fused PET-CT images and corrected for blood-pool activity using the maximum tissue-to-background ratio (TBR_{max}). Aortic atherosclerotic burden was quantified by CT wall thickness, plaque volume and calcium scoring.

2

Results

18F-Fluciclatide uptake co-localised with regions of increased $\alpha_v\beta_3$ integrin expression, and markers of inflammation and angiogenesis. 18F-Fluciclatide vascular uptake was confirmed *in vivo* using kinetic modeling, and on static imaging correlated with measures of aortic atherosclerotic burden: wall thickness (r=0.57, p=0.001), total plaque volume (r=0.56, p=0.001) and aortic CT calcium score (r=0.37, p=0.01). Patients with recent myocardial infarction had greater aortic 18F-fluciclatide uptake than those with stable disease (TBR_{max} 1.33 vs 1.21, p=0.01).

Conclusions

In vivo expression of $\alpha_v\beta_3$ integrin in human aortic atheroma is associated with plaque burden and is increased in patients with recent myocardial infarction. Quantification of $\alpha_v\beta_3$ integrin expression with 18F-fluciclatide PET has potential to assess plaque vulnerability and disease activity in atherosclerosis.

Keywords

Atherosclerosis; positron emission tomography; integrin; computed tomography

Key Questions

What is already known about this subject?

The $\alpha_v\beta_3$ integrin receptor is a mediator of plaque angiogenesis and inflammation and has been targeted as a potential marker of atherosclerotic activity using PET radiotracers. As yet however, studies of $\alpha_v\beta_3$ integrin-specific radiotracers in humans are lacking.

What does this study add?

This is the largest study to date assessing $\alpha_v\beta_3$ integrin expression in human atherosclerosis. We have demonstrated that 18F-fluciclatide uptake localises to vascular inflammation and angiogenesis, correlates with plaque burden and is increased in patients with clinically unstable disease.

How might this impact on clinical practice?

Non-invasive markers of atherosclerotic disease activity may identify vulnerable patients and provide incremental risk prediction to current anatomic imaging approaches. In this study, 18F-fluciclatide shows promise as a non-invasive marker of disease activity and instability in atherosclerosis.

4

Introduction

Atherosclerotic cardiovascular disease is the commonest cause of death worldwide, and elucidating the mechanisms underlying the propagation and rupture of atherosclerotic plaques remains a key public health goal.(1) Although our understanding of the pathogenesis underlying atherosclerosis has progressed over the last two decades, accurate prediction of clinical events remains elusive. There is therefore considerable interest in non-invasive imaging techniques that go beyond the detection of luminal stenoses and instead focus on measuring disease activity within the vasculature.(2,3)

Combined positron emission tomography (PET) and computed tomography (CT) is a non-invasive hybrid imaging technique that integrates targeted functional molecular imaging with high-detail anatomical definition. This technique has been used to quantify vascular inflammation and calcification activity with success in both carotid and coronary atherosclerosis.(4-7) Recently, intraplaque angiogenesis and neovascularization has emerged as a key factor in the development, progression, and instability of atherosclerotic plaques.(8) The integrin $\alpha_v\beta_3$ cell surface receptor is upregulated on endothelial cells in states of angiogenesis and is also observed on macrophages at sites of increased vascular inflammation, another key contributor to plaque instability. This receptor helps coordinate interaction between cellular components and the extra-cellular matrix, and contains a distinctive RGD-amino acid sequence (the arginine-glycine-aspartate motif) in the cell-ligand interaction site. On this basis, several PET tracers targeting the RGD sequence

have been developed for monitoring angiogenesis in malignant tumours.(9,10)

These tracers have also shown promise in monitoring atherosclerotic activity in

pre-clinical models (8,11-14) and in a recent small study of patients with carotid

atheroma.(7)

18F-Fluciclatide is a novel RGD-based PET radiotracer with high affinity for the

$\alpha_v\beta_3$ integrin receptor.(10,15,16) We hypothesized that 18F-fluciclatide may act

as an imaging marker of atherosclerotic disease activity *in vivo*, informing about

both inflammation and angiogenesis. In this study, we sought to characterize

the cellular and imaging characteristics of 18F-fluciclatide uptake in human

atherosclerosis using a clinical cohort of patients with both stable and unstable

clinical disease.

6

Methods

Study populations

In total we studied 50 patients. Four patients were recruited who had sustained a recent stroke and were undergoing carotid endarterectomy. In these patients, excised carotid plaques were examined using histology and 18F-fluciclatide autoradiography. For *in vivo* imaging, 46 patients were recruited from the Royal Infirmary of Edinburgh between July 2013 and December 2014. This cohort comprised 19 *unstable* patients with a recent acute ST-segment elevation myocardial infarction (MI) (14±7 days after MI) (NCT01813045),(17) and 27 *stable* patients with either stable angina (n=6) or asymptomatic atherosclerotic disease (n=21; 12 had calcific aortic valve disease) (NCT01837160). Exclusion criteria were age <40 years, women of childbearing potential, severe renal failure (estimated glomerular filtration rate <30 mL/min) or hepatic failure (Childs-Pugh grade B or C), atrial fibrillation, known contrast allergy, inability to undergo scanning and inability to provide informed consent. All 46 subjects underwent 18F-fluciclatide PET imaging alongside clinical assessment that included evaluation of cardiovascular risk and high sensitivity C-reactive protein (hs-CRP) measurement (Biocheck inc.; Foster City, California).

Studies were approved by the local research ethics committee and conducted in accordance with the Declaration of Helsinki and with written informed consent of each participant.

Radiosynthesis of 18F-Fluciclatide

18F-Fluciclatide was manufactured at the Clinical Research Imaging Centre on an automated module (FASTlab synthesiser; GE Healthcare) by coupling an amino-oxy-functionalized peptide precursor (AH111695) with 4-18F-fluorobenzaldehyde at pH 3.5 to form 18F-fluciclatide.(17) A full description of this synthesis has been published previously.(16)

Histological Validation

Carotid endarterectomy specimens (Data Supplement) were fresh frozen and sectioned in cryosection medium. Both atheromatous and non-atheromatous segments were fixed, stained with hematoxylin-eosin (HE) and examined by immunohistochemistry for smooth muscle actin, CD31, CD68, and $\alpha_v\beta_3$ integrin receptor expression before digital image capture (Axioscan.Z1, Zeiss, UK). Image analysis was performed on ImageJ32 software (NIH, Bethesda, Maryland). Staining was expressed as a percentage of the total plaque area and with an object size set threshold applied at 20 x 10 pixels, to limit counting to cell-sized objects. The density of cell staining in the endarterectomy tissue was expressed as cells per mm^2.(18)

Autoradiography was performed to identify the precise localization of 18F-fluciclatide binding in atherosclerotic tissue. Carotid sections were bathed in a solution of 18F-fluciclatide (1 kBq/mL) for 60 min and rinsed with phosphate buffer solution. To rule out non-specific radiotracer uptake, an un-labeled highly concentrated solution of fluciclatide was added to bind competitively with the $\alpha_v\beta_3$ integrin receptors. 18F-Fluciclatide binding was imaged using a FujiFilm

FLA-5100 Fluorescent Image Analyser (Raytek Scientific Limited, Sheffield, UK).

Clinical 18F-Fluciclatide PET Imaging

All patients in the imaging cohort underwent PET-CT imaging of the thorax with a hybrid scanner (Biograph mCT, Siemens Medical Systems, Erlangen, Germany) at the Clinical Research Imaging Centre, University of Edinburgh. Subjects were administered a target dose of 230 MBq 18F-fluciclatide. An attenuation correction CT scan (non-enhanced 120 kV and 50 mA, 3-mm slices) was performed prior to PET acquisition. To define tracer pharmacodynamics and the optimum timing of scanning, dynamic PET imaging of the thorax was performed in the initial 20 patients in 3-dimensional mode using a single bed position for 70 min. For the remainder of the study subjects, static imaging was performed at the optimal time point (found to be 40 min post-injection) using a single 30-min bed position in list mode with electrocardiographic gating. Immediately after PET acquisition, thoracic CT angiography was performed. (Data Supplement)

PET Image Reconstruction and Analysis

Kinetic analysis was performed on the dynamic PET studies to investigate the pharmacodynamics of 18F-fluciclatide uptake within atheroma. The methodology is described in detail in the data supplement. In all patients, static electrocardiogram-gated PET images were reconstructed in diastole (40-70 min post-injection, 50–75% of the R-R interval, Ultra-HD, 2 iterations, 21 subsets, zoom x2, 200 pixels). Images were analyzed by experienced observers blinded to the demographic data (WJ, AV) using an OsiriX

workstation (OsiriX version 6.0 64-bit; OsiriX Imaging Software, Geneva, Switzerland). PET images were fused with the attenuation correction CT, and regions of interest (ROIs) drawn around the thoracic aorta on serial axial slices just beyond the discernible adventitial border. Aortic uptake was assessed in three regions: the ascending thoracic aorta (from the level of mid-right pulmonary artery (RPA) up to the last slice where the aorta maintained its circular cross-sectional appearance), the descending thoracic aorta (the region extending from the tip of the diaphragm up to the last circular slice) and the aortic arch (the region of the aorta connecting the ascending and descending aorta). Within these regions, mean and maximum tracer activities were measured using standard uptake values (SUV; the decay corrected tissue concentration of the tracer divided by the injected dose per body weight, kBq/mL) and corrected for mean radiotracer blood pool activity to provide a mean of the maximum tissue-to-background ratio (mean TBR_{max}).(5,19-20) The blood pool radiotracer activity was quantified in the superior vena cava (SVC), measured in the axial plane on 4-5 sequential 5-mm axial slices above the level of the junction of the left innominate vein. In a sub-study of 10 randomly selected subjects, images were assessed independently by two experienced observers and the inter-observer reproducibility of 18F-fluciclatide SUV and TBR measurements assessed.

CT Image Reconstruction and Analysis

The aortic CT calcium score was calculated for the aorta as a whole and for its different regions using axial slices on the attenuation correction CT dataset

(OsiriX version 6.0 64-bit; OsiriX Imaging Software, Geneva, Switzerland) and expressed in arbitrary units (AU).(21) In those patients whose descending aorta was visualised within contrast CT datasets (n=33), further measures of aortic atherosclerotic plaque burden were made on dedicated plaque analysis software (Vital Images, Minnetonka, Minnesota, USA). Using the sagittal plane, the entire portion of the descending thoracic aorta within the field of contrast CT acquisition was delineated and the luminal blood pool removed using semi-automated thresholding. The mean aortic wall thickness was recorded and corrected for the vessel diameter providing the indexed wall thickness. Additionally, the aortic wall volume was recorded and corrected for total vessel volume to provide an indexed plaque volume.

Statistical analysis

Continuous data were tested for normality visually and with the D'Agostino and Pearson Omnibus test. Continuous parametric variables were expressed as mean±standard deviation and compared using Pearson correlation. Non-parametric data were presented as median [interquartile range] and compared using Spearman correlation or Wilcoxon signed-rank test as appropriate. Aortic calcium score and hs-CRP were log-transformed to base 10 to achieve normality prior to statistical analysis. Interobserver reproducibility was calculated by Bland Altman method and presented as mean bias ± 2 standard deviations, and intraclass correlation coefficients (ICC).(22) Student's *t*-test or Mann-Whitney U test was used for analysis of categorical variables. Statistical analysis was performed with Graph Pad Prism version 6 (GraphPad Software Inc., California USA). A two-sided P<0.05 was taken as statistically significant.

Results

Plaque Autoradiography and Histology

Autoradiography of carotid plaque demonstrated focal 18F-fluciclatide binding in regions of advanced atherosclerosis that was effectively blocked by unlabeled fluciclatide (Figure 1 A and B). On adjacent tissue sections processed for histology, these regions of *ex vivo* 18F-fluciclatide uptake co-localised with areas of intense cellular staining of $\alpha_v\beta_3$ integrin (45.2 [29.1-66.9] cells/mm^2, % area 4.2 [3.2-5.7]), microvascular endothelial cells at sites of angiogenesis and positive remodeling (CD31+; 23.0 [6.5-63.0] cells/mm^2, % area 2.5 [2.2-4.9]), and inflammatory macrophages deeper adjacent to the necrotic core (CD68+; 32.0 [21.0-49.8] cells/mm^2, % area 3.7 [2.4-5.6], Figure 1 C-H). By comparison regions of carotid endarterectomy specimen without visible atheroma did not demonstrate 18F-fluciclatide uptake, and had much lower levels of $\alpha_v\beta_3$ integrin receptor expression (4.5 [4.3-5.2] cells/mm^2, % area 0.6 [0.5-2.0], both p=0.05 compared to areas with increased 18F-fluciclatide expression), as well as staining for both angiogenic endothelial cells (CD31+; 2.1 [1.8-2.4] cells/mm^2, % area 0.9 [0.6-1.2], both p=0.05) and inflammatory macrophages (CD68+; 4.3 [2.8-4.4] cells/mm^2, % area 0.6 [0.5-1.2], both p=0.03).

In Vivo Imaging Cohort

A total of 46 subjects underwent PET imaging with CT angiography (age 66±10 years, 74% male; Table 1) following injection of 226±13 mBq 18F-fluciclatide. Of the 46 subjects recruited, 19 had suffered a recent MI (*unstable cohort*), and 27 had imaging evidence of aortic atherosclerosis on CT but no recent cardiovascular events (*stable cohort*: 6 with stable angina and 21 with sub-

clinical disease who were asymptomatic with no prior cardiovascular events). Interestingly, those in the stable cohort had greater aortic calcification than patients in the unstable group (AU [IQR]; 326 [11-1114] vs 19 [0-483], p<0.01), reflecting their greater age (years; 70±8 vs 61±12, p<0.01). The groups were well matched for gender (p=0.97) and body-mass index (p=0.25), and were both characterized by high prevalence of atherosclerotic risk factors, with more smokers in the unstable group (p=0.02) and more patients with hypertension in the stable group (p=0.001). No adverse events were reported following administration of 18F-fluciclatide and the average total radiation dose per participant was 15 mSv.

Dynamic Analysis of Aortic 18F-Fluciclatide Uptake

On kinetic analysis (n=20), activity within aortic atheroma increased gradually, reaching a plateau at 40–70 min. Injected 18F-fluciclatide activity has a biexponential blood pool clearance with a half-life of about 10 min consisting of a fast redistribution component with a slower clearance component, causing relatively high residual blood pool activity during PET acquisition (40-70 min post-injection, SVC SUV_{mean} 2.74±0.49; Figure 2). Consequently, whilst 18F-fluciclatide uptake in aortic atheroma was measurable above background, tissue-to-background ratios were relatively low (TBR_{max} range 1.08-1.68; Tables 2 and 3, Figures 2 and 3). In the 3-D Patlak slope (Ki) parametric images, 6 datasets (30%) were uninterpretable due to patient movement. In the remaining studies, increased aortic 18F-fluciclatide uptake was observed in half of subjects. Patlak modelling demonstrated a discernible linear phase suggesting irreversible ligand-receptor binding over the selected acquisition

time and a greater Ki slope in these subjects compared to patients with no aortic uptake (Figure 2). Subjects with uptake present on Patlak analysis (n=7) also appeared to have higher 18F-fluciclatide uptake on standard analysis (TBR$_{max}$ 1.32±0.05 vs 1.19±0.03, p=0.08) and greater aortic calcification (aortic calcium score 704 [28-1788] vs 0 [0-119] AU, p=0.06) than those without visible uptake, although this did not reach statistical significance.

Aortic 18F-Fluciclatide Uptake Reproducibility Studies

Using static PET images, quantification of 18F-fluciclatide blood-pool activity demonstrated excellent interobserver reproducibility, with no fixed or proportional bias (SUV$_{mean}$ mean difference; -0.11 [-0.36 – 0.15]) and a good intraclass correlation co-efficient (0.95, Table S1). Quantification of aortic 18F-fluciclatide uptake using the established mean TBR$_{max}$ approach (5,20) also displayed no fixed or proportional bias (mean difference; 0.08 [-0.01–0.16]) with good intra-class correlation (0.92) (Table S1).

Aortic 18F-Fluciclatide Uptake and Atheroma Burden

Our study cohort comprised patients with a wide spectrum of aortic atherosclerotic burden (aortic calcium score range 0-6857 AU). On static PET images, aortic 18F-fluciclatide uptake demonstrated a moderate relationship with disease burden in the aorta using both CT calcium scoring (r=0.37 [0.08-0.60], p=0.01) and the indexed plaque volume (r=0.56 [0.26-0.75]; p<0.001) (Table 3, Figures 3 and 4). A good correlation was also observed with the relative vessel wall thickness (expressed as a percentage of vessel diameter, r=0.57 [0.28-0.76]; p<0.001). There was no correlation between aortic 18F-

fluciclatide uptake and the inflammatory marker C-reactive protein ($\log_{10}$ hs-CRP r=0.18, p=0.28).

Aortic 18F-Fluciclatide Uptake in Stable and Unstable Patients

To establish whether 18F-fluciclatide uptake may be a marker of unstable atherosclerotic activity, we compared aortic uptake in patients who had sustained a recent MI to those in our stable cohort. Given the association demonstrated between 18F-fluciclatide activity and plaque burden, we matched patients in the two groups according to CT calcium score (Table S2). We demonstrated increased 18F-fluciclatide aortic uptake in patients with recent MI compared to those in the stable cohort (TBR_{max}; 1.33±0.15vs 1.21±0.1, p=0.008) despite equivalent aortic calcium scores (Table 2, Figure 4). Moreover, in patients with recent MI, a stronger correlation was observed between aortic plaque burden and 18F-fluciclatide uptake than in the patient population as a whole (aortic wall thickness r=0.68, p=0.02). When aortic SUV measurement were assessed, these were consistently increased in the unstable groups compared to the stable groups across all regions of the aorta, even before attempts were made to match these groups by calcium score (p<0.05 for all aortic regions, Table 2 and S3).

Aortic 18F-Fluciclatide and Cardiovascular Risk Factors

Amongst patients in the stable cohort, aortic 18F-fluciclatide uptake correlated with a number of risk factors (Table 3). 18F-Fluciclatide activity was higher in patients with hypercholesterolemia compared to those without (1.37±0.04 vs 1.24±0.06, p=0.007). Apparent observed trends were also seen in patients with diabetes (1.41±0.08 vs 1.28±0.02, p=0.06) and those with a diagnosis of

1
2
3
4
5
6
7
8
9
10
11
12
13
14
15
16
17
18
19
20
21
22
23
24
25
26
27
28
29
30
31
32
33
34
35
36
37
38
39
40
41
42
43
44
45
46
47
48
49
50
51
52
53
54
55
56
57
58
59
60

coronary heart disease (1.37±0.04 vs 1.28±0.03, p=0.08), although these did not meet statistical significance. Again, a strong correlation was observed between 18F-fluciclatide uptake and the CT calcium score (*r*=0.62, p<0.001) in this subgroup.

Discussion

We present the largest multimodality imaging study to date evaluating the application of an RGD-based $\alpha_v\beta_3$ integrin receptor radiotracer in the assessment of human atheroma. We have demonstrated that *ex vivo* 18F-fluciclatide binding co-localises to sites of $\alpha_v\beta_3$ integrin receptor expression in excised carotid plaques, and this was associated with regions of both angiogenesis and inflammation. We have further demonstrated *in vivo* that 18F-fluciclatide uptake increased with progressive atherosclerotic plaque burden and is higher in patients with unstable versus stable atherosclerotic disease. These data would suggest that 18F-fluciclatide holds promise as a non-invasive marker of disease activity in atherosclerosis, informing us about two key characteristics of high-risk atheroma: inflammation and angiogenesis. RGD-based tracers may therefore aid our pathophysiological understanding of this important condition and help identify patients at increased risk of adverse cardiovascular events.

Plaque inflammation and angiogenesis are two key pathological processes associated with atheroma progression, plaque rupture and clinical events. Macrophages drive expansion of the necrotic core and secrete matrix metalloproteinases that weaken the fibrous cap, predisposing it to rupture. Angiogenesis is believed to occur in response to hypoxic conditions within the necrotic core and is associated with high-risk plaque characteristics.(3) In addition, these new vessels are prone to leakage and rupture resulting in plaque hemorrhage that itself results in an pro-inflammatory response, plaque destabilization and clinical events. A non-invasive imaging technique that can

inform about the activity of these two adverse pathological processes might therefore be useful in identifying patients with active high-risk atheroma. Indeed, it is hoped that non-invasive markers of systemic atherosclerotic disease activity may identify the vulnerable patient and provide incremental risk prediction to an assessment of radiographic coronary or carotid disease burden alone.(2,23) We have here demonstrated that 18F-fluciclatide PET-CT is an emerging and promising approach to achieve these aims.

Our autoradiographic data showed focal 18F-fluciclatide binding within carotid atheroma that localised histologically to $\alpha_v\beta_3$ integrin expression with no evidence of non-specific binding. Regions of 18F-fluciclatide uptake on autoradiography also corresponded to sites of immunohistochemical cellular staining for vascular endothelial cells and macrophages. This is in keeping with previous RGD-radiotracer studies and supports its role as a selective marker for angiogenic and inflammatory components of atherosclerotic activity.(7, 24,25) Due to the close relationship between intraplaque inflammation and angiogenesis however, we are unable to ascertain whether 18F-fluciclatide was binding preferentially to one or the other of these processes.

Dynamic *in vivo* imaging studies in 20 subjects confirmed irreversible 18F-fluciclatide binding to regions of aortic atherosclerosis over the selected acquisition time, and demonstrated that the optimum time for 18F-fluciclatide imaging in the aorta is between 40 and 70 min. This timeframe was used for subsequent static PET imaging across the cohort as a whole. Static *in vivo* imaging demonstrated reproducible quantification of 18F-fluciclatide in aortic

atheroma of all 46 patients, and this was correlated with the severity of aortic atherosclerotic burden, itself a manifestation of systemic atherosclerosis and a strong predictor of cardiovascular events.(26,27) Indeed associations were observed with the aortic calcium score, aortic wall thickness and overall plaque volume. In patients with clinically stable disease, aortic uptake of 18F-fluciclatide was increased in subjects with hypercholesterolemia with trends towards higher uptake in patients with diabetes mellitus and those with ischemic heart disease that did not meet statistical significance. Perhaps most importantly, 18F-fluciclatide uptake in aortic atheroma was increased in patients with unstable (recent MI) versus stable clinical disease. Interestingly, using 18F-fluorodeoxyglucose, we have previously demonstrated a similar pattern of increased metabolic activity in aortic atheroma amongst patients with recent MI.(28) These data therefore lend support to the hypothesis that acute MI causes inflammation and instability in systemic atherosclerosis, as has been suggested in preclinical murine models.(29) It also provides further validity to the concept that 18F-fluciclatide uptake can identify higher risk plaques. However, whether this increased disease activity truly represents a response to the infarct or rather the underlying trigger remains to be determined.

We acknowledge that there are some limitations of our study that include potential partial volume artefacts, a limited histological assessment and the use of surrogate measures for aortic histology. 18F-Fluciclatide imaging prior to carotid endarterectomy would allow for a more direct comparison between *in-vivo* imaging and histological assessment and consolidate our findings in line with previous publications.(7) Furthermore, our exploratory assessment of

aortic plaque volume may not take into account non-atheromatous intimal thickening in response to chronic hypertension. The dynamic imaging approach proved sensitive to patient movement during the prolonged acquisition period, limiting its utility in quantitative analysis, but this may ultimately be readdressed by novel motion tracking systems that allow for correction of cardiac and respiratory motion, enabling even greater definition of regional $\alpha_v\beta_3$ integrin expression.(30) Nonetheless, we believe that the totality of our comprehensive evidence using multiple approaches and imaging modalities provides a robust and cogent argument to support our findings.

In conclusion, this is the largest study to date assessing $\alpha_v\beta_3$ integrin expression in human atherosclerotic disease. We have demonstrated that 18F-fluciclatide uptake localises to regions of inflammation and angiogenesis, correlates with the plaque burden and is increased in patients with clinically unstable disease. Although further study is required, our data indicate that 18F-fluciclatide shows promise as a non-invasive marker of disease activity and instability in atherosclerosis.

Acknowledgements and Funding

Clinical Trials Registration

Unique Identifiers: NCT01813045, NCT01837160

https://clinicaltrials.gov/ct2/show/NCT01813045,

https://clinicaltrials.gov/ct2/show/NCT01837160

The Corresponding Author has the right to grant on behalf of all authors and does grant on behalf of all authors, an exclusive licence (or non exclusive for government employees) on a worldwide basis to the BMJ Publishing Group Ltd and its Licensees to permit this article (if accepted) to be published in HEART editions and any other BMJPGL products to exploit all subsidary rights

References

1.   Mozaffarian D, Benjamin EJ, Go AS, Arnett DK, Blaha MJ, Cushman M, et al. Heart Disease and Stroke Statistics-2015 Update. Circulation. 2014 Dec 17.

2.   Dweck MR, Aikawa E, Newby DE, Rudd JHF, Narula J, Fayad ZA. Non-Invasive Molecular Imaging of Disease Activity. Circulation Research. 2016 Jul 8;119(2):330-40.

3.   Dweck MR, Doris MK, Motwani M, Adamson PD, Slomka P, Dey D, et al. Imaging of coronary atherosclerosis - evolution towards new treatment strategies. Nat Rev Cardiol. 2016 Sep;13(9):533–48.

4.   Rudd JHF, Myers KS, Bansilal S, Machac J, Rafique A, Farkouh M, et al. 18Fluorodeoxyglucose Positron Emission Tomography Imaging of Atherosclerotic Plaque Inflammation Is Highly Reproducible. J Am Coll Cardiol. 2007 Aug;50(9):892–6.

5.   Joshi NV, Vesey AT, Williams MC, Shah ASV, Calvert PA, Craighead FHM, et al. (18)F-fluoride positron emission tomography for identification of ruptured and high-risk coronary atherosclerotic plaques: a prospective clinical trial. Lancet. 2014 Nov;383(9918):705–713.

6.   Dweck MR, Chow MWL, Joshi NV, Williams MC, Jones C, Fletcher AM, et al. Coronary Arterial 18F-Sodium Fluoride Uptake. J Am Coll Cardiol. 2012 Apr 24;59(17):1539–48.

7.   Beer AJ, Pelisek J, Heider P, PET/CT Imaging of Integrin αvβ3 expression in human carotid atherosclerosis. J Am Coll Cardiol Imaging; 2014 Feb;7(2):178-87.

8.   Kate ten GL, Sijbrands EJG, Valkema R, Cate ten FJ, Feinstein SB, Steen AFW, et al. Molecular imaging of inflammation and intraplaque vasa vasorum: A step forward to identification of vulnerable plaques? J Nucl Cardiol. 2010 Jun 15;17(5):897–912.

9.   Mena E, Owenius R, Turkbey B, Sherry R, Bratslavsky G, Macholl S, et al. [18F]Fluciclatide in the in vivo evaluation of human melanoma and renal tumors expressing αvβ3 and αvβ5 integrins. Eur J Nucl Med Mol Imaging. 2014 Jun 28;41(10):1879–88.

10.   Kenny LM, Coombes RC, Oulie I, Contractor KB, Miller M, Spinks TJ, et al. Phase I trial of the positron-emitting Arg-Gly-Asp (RGD) peptide radioligand 18F-AH111585 in breast cancer patients. Journal of Nuclear Medicine. 2008 Jun;49(6):879–86.

11.   Yoo JS, Lee J, Jung JH, Moon BS, Kim S, Lee BC, et al. SPECT/CT Imaging of High-Risk Atherosclerotic Plaques using Integrin-Binding RGD Dimer Peptides. Sci Rep. 2015;5:11752.

12. Su H, Gorodny N, Gomez LF, Gangadharmath UB, Mu F, Chen G, et al. Atherosclerotic plaque uptake of a novel integrin tracer ^{18}F-Flotegatide in a mouse model of atherosclerosis. J Nucl Cardiol. 2014 Jun;21(3):553–62.

13. Vancraeynest D, Roelants V, Bouzin C, Hanin F-X, Walrand S, Bol V, et al. αVβ3 integrin-targeted microSPECT/CT imaging of inflamed atherosclerotic plaques in mice. EJNMMI Res. 2016 Dec;6(1):29.

14. Laitinen I, Saraste A, Weidl E, Poethko T, Weber AW, Nekolla SG, et al. Evaluation of αvβ3 Integrin-Targeted Positron Emission Tomography Tracer 18F-Galacto-RGD for Imaging of Vascular Inflammation in Atherosclerotic Mice. Circ Cardiovasc Imaging. 2009;2:331–8.

15. Tomasi G, Kenny L, Mauri F, Turkheimer F, Aboagye EO. Quantification of receptor-ligand binding with [18F]fluciclatide in metastatic breast cancer patients. Eur J Nucl Med Mol Imaging. 2011 Sep 3;38(12):2186–97.

16. McParland BJ, Miller MP, Spinks TJ, Kenny LM, Osman S, Khela MK, et al. The biodistribution and radiation dosimetry of the Arg-Gly-Asp peptide 18F-AH111585 in healthy volunteers. Journal of Nuclear Medicine. 2008 Oct;49(10):1664–7.

17. Jenkins WS, Vesey AT, Stirrat C, Connell M, Lucatelli C, Neale A, et al. Cardiac αvβ3 integrin expression following acute myocardial infarction in humans. Heart. 2017 Apr; 103(8): 607–615.

18. Dweck MR, Jenkins WSA, Vesey AT, Pringle MAH, Chin CWL, Malley TS, et al. 18F-NaF Uptake Is a Marker of Active Calcification and Disease Progression in Patients with Aortic Stenosis. Circulation: Cardiovascular Imaging. 2014 Feb 7.

19. Niccoli Asabella A, Ciccone MM, Cortese F, Scicchitano P, Gesualdo M, Zito A, et al. Higher reliability of 18F-FDG target background ratio compared to standardized uptake value in vulnerable carotid plaque detection: a pilot study. Ann Nucl Med. 2014 Jul;28(6):571–9.

20. Dweck MR, Jones C, Joshi NV, Fletcher AM, Richardson H, White A, et al. Assessment of Valvular Calcification and Inflammation by Positron Emission Tomography in Patients With Aortic Stenosis. Circulation. 2012 Jan 3;125(1):76–86.

21. Dweck MR, Khaw HJ, Sng GKZ, Luo ELC, Baird A, Williams MC, et al. Aortic stenosis, atherosclerosis, and skeletal bone: is there a common link with calcification and inflammation? European Heart Journal. 2013 Feb 7.

22. Bland JM, Altman DG. Statistical methods for assessing agreement between two methods of clinical measurement. Lancet. 1986 Feb 8;1(8476):307–10.

23.   Arbab-Zadeh A, Fuster V. The Myth of the "Vulnerable Plaque":
      Transitioning From a Focus on Individual Lesions to Atherosclerotic
      Disease Burden for Coronary Artery Disease Risk Assessment. J Am
      Coll Cardiol. 2015 Mar 3;65(8):846–55.

24.   Golestani R, Mirfeizi L, Zeebregts CJ, Westra J, de Haas HJ,
      Glaudemans AWJM, et al. Feasibility of [18F]-RGD for ex vivo imaging
      of atherosclerosis in detection of αvβ3 integrin expression. J Nucl
      Cardiol. 2015 Feb 20.

25.   Sun Y, Zeng Y, Zhu Y, Feng F, Xu W, Wu C, et al. Application of
      (68)Ga-PRGD2 PET/CT for αvβ3-integrin imaging of myocardial
      infarction and stroke. Theranostics. 2014;4(8):778–86.

26.   Hong SN, Gona P, Fontes JD, Oyama N, Chan RH, Kenchaiah S, et al.
      Atherosclerotic biomarkers and aortic atherosclerosis by cardiovascular
      magnetic resonance imaging in the Framingham Heart Study. J Am
      Heart Assoc. 2013;2(6).

27.   Dutta P, Courties G, Wei Y. Aortic Calcified Plaques and Cardiovascular
      Disease (The Framingham Study). 2004 Mar 15; 1–5.

28.   Joshi NV, Toor I, Shah ASV, Carruthers K, Vesey AT, Alam SR, et al.
      Systemic Atherosclerotic Inflammation Following Acute Myocardial
      Infarction: Myocardial Infarction Begets Myocardial Infarction. J Am
      Heart Assoc. 2015 Sep;4(9):e001956.

29.   Dutta P, Courties G, Wei Y, Leuschner F, Gorbatov R, Robbins CS, et
      al. Myocardial infarction accelerates atherosclerosis. Nature. 2012 Jun
      27;487(7407):325–9.

30.   Rubeaux M, Joshi N, Dweck MR, Fletcher A, Motwani M, Thomson LE,
      et al. Motion correction of 18F-sodium fluoride PET for imaging
      coronary atherosclerotic plaques. J Nucl Med. 2015 Oct 15.

24

Table 1. Patient Characteristics

	All (n=46)	Stable Atherosclerosis (n=27)	Unstable Atherosclerosis (n=19)	P value*
Age (years)	66±10	70±8	61±12	0.006
Male Sex	34 (74)	20 (74)	14 (74)	0.97
BMI (kg/m^2)	28±4	28±4	29±5	0.25
Systolic BP (mmHg)	140±22	149±19	127±19	<0.001
18F-Fluciclatide dose (MBq)	226±13	225±13	228±14	0.62
Cardiovascular History				
Angiographically documented CAD	26 (57)	7 (26)	19 (100)	<0.001
Prev MI	24 (52)	5 (19)	19 (100)	<0.001
Prev PCI	20 (43)	2 (7)	18 (95)	<0.001
Prev CVD	4 (11)	4 (14)	0 (0)	0.08
Risk Factors				
Current smoker	9 (20)	1 (4)	8 (42)	0.001
Diabetes Mellitus	6 (13)	4 (14)	2 (10)	0.58
Prior hypertension	23 (50)	18 (67)	6 (32)	0.02
Prior Hypercholester-olemia	25 (54)	12 (44)	12 (63)	0.21
hs-CRP (mg/l)	3.5 [1.4-7.8]	2.7 [1.4-5.8]	5.6 [2.0-11.7]	<0.001
Log$_{10}$ hs-CRP (mg/l)	0.51±0.51	0.41±0.44	0.65±0.56	<0.001
Medications				
Aspirin	28 (61)	10 (37)	19 (100)	<0.001
Clopidogrel	19 (41)	4 (14)	19 (100)	<0.001
Statin	31 (67)	13 (48)	19 (100)	<0.001
β-Blocker	27 (59)	8 (30)	19 (100)	<0.001
ACEi/ARB	31 (67)	10 (37)	18 (95)	<0.001
Calcium Channel Blocker	7 (15)	6 (22)	1 (5)	0.11

Categorical data are displayed as n (%). Normally distributed data displayed as mean±SD. Non-normally distributed data displayed as median [interquartile range]. IHD - ischemic heart disease; AS - aortic stenosis; CAD - coronary artery disease; MI - myocardial infarction; CVD – cerebrovascular disease; PCI - percutaneous coronary intervention; hs-CRP - high sensitivity c-reactive protein; ACEi - ACE-inhibitor; ARB - Angiotensin Receptor Blocker.

*P-values are quoted for comparisons between matched stable and unstable groups.

Table 2. Imaging Results

	All (n=46)	Stable Atherosclerosis (n=27)	Matched Stable Atherosclerosis (n=19) $^\Psi$	Unstable Atherosclerosis (n=19)	P value[*]
18F-Fluciclatide PET uptake					
SVC (SUV_{mean})	2.74±0.49	2.62±0.46	2.54±0.40	2.9±0.48	0.02
Whole aorta (*mean SUV_{max}*)	3.59±0.62	3.40±0.62	3.19±0.65	3.84±0.55	0.001
Whole aorta (*mean TBR_{max}*)	1.32±0.14	1.30±0.12	1.26±0.09	1.33±0.18	0.14
Ascending aorta (*mean TBR_{max}*)	1.32±0.16	1.31±0.17	1.25±0.10	1.34±0.17	0.05
Aortic Arch (*mean TBR_{max}*)	1.30±0.14	1.26±0.14	1.21±0.1	1.33±0.15	0.008
Descending aorta (*mean TBR_{max}*)	1.32±0.17	1.32±0.13	1.29±0.11	1.33±0.21	0.56
CT Calcium Score					
Whole aorta (*AU*)	95 [0-852]	326 (11-1114)	36 (0-469)	19 [0-483]	0.85
Ascending aorta (*AU*)	0 [0-11]	0 (0-46)	0 (0-0)	0 [0-0}	0.15
Aortic arch (*AU*)	29 [0-352]	102 (0-586)	13 (0-469)	0 [0-263]	0.76
Descending aorta (*AU*)	7.5 [0-78]	0 (0-123)	0 (0-123)	8 [0-71]	0.43
CTA Plaque analysis (descending aorta)					
Mean wall thickness (*% vessel diameter*)	10.3±4.9	8.4±2.8	8.4±3.1	14.0±6.3	0.003
Plaque burden (*% total volume*)	9.1±3.9	7.7±2.3	7.7±2.5	12.0±4.7	0.004

$^\Psi$ *Stable group subjects paired to equivalent calcium score in unstable group.*
[*] *P-values are quoted for comparisons between matched stable and unstable groups.*

SUV - standard uptake value; SVC – superior vena cava; TBR - tissue-to-background ratio

Table 3. PET uptake and baseline characteristics

	Total Aortic 18F-Fluciclatide Uptake		
	All patients	Stable Cohort	Unstable Cohort
Continuous variables			
CT calcium score (Log^{10}AU)	r=0.37 (0.08-0.60) p=0.01	r=0.62 (0.43-0.81) p<0.001	r=0.20 (-0.28-0.60) p=0.41
Mean wall thickness (% vessel diameter) [Ψ]	r=0.57 (0.28-0.76) p<0.001	r=0.18 (-0.26-0.56) p=0.43	r=0.69 (0.15-0.91) p=0.02
Plaque volume (% total volume) [Ψ]	r=0.56 (0.26-0.75) p<0.001	r=0.16 (-0.28-0.55) p=0.47	r=0.68 (0.13-0.90) p=0.02
Log$_{10}$ hs-CRP (mg/l)	r=0.18 (-0.14-0.46) p=0.28	r=0.32 (-0.07-0.62) p=0.10	r=-0.24 (-0.63-0.24) p=0.06
Categorical variables			
Hypertension (mean TBR$_{max}$)	1.31±0.05 vs 1.32±0.04 p=0.66	1.31±0.05 vs 1.32±0.04 p=0.66	
Established Ischemic Heart Disease (mean TBR$_{max}$)	1.34±0.06 vs 1.28±0.06 0.15	1.37±0.04 vs 1.28±0.03 0.08	
Hypercholesterolemia (mean TBR$_{max}$)	1.34±0.06 vs 1.28±0.06 p=0.16	1.37±0.04 vs 1.24±0.06 p=0.007	
Diabetes mellitus (mean TBR$_{max}$)	1.40±0.10 vs 1.30±0.05 p=0.15	1.41±0.08 vs 1.28±0.02 p=0.06	
Current Smokers (mean TBR$_{max}$)	1.36±0.10 vs 1.30±0.04 p=0.30	*N* too small	

[Ψ]18F-Fluciclatide uptake assessed in the descending aorta only, to correspond with CT analysis.
CT – computed tomography; hs-CRP - high sensitivity C-reactive protein

1
2
3
4
5
6
7
8
9
10
11
12
13
14
15
16
17
18
19
20
21
22
23
24
25
26
27
28
29
30
31
32
33
34
35
36
37
38
39
40
41
42
43
44
45
46
47
48
49
50
51
52
53
54
55
56
57
58
59
60

Figure 1. 18F-Fluciclatide Uptake in Carotid Atheroma

(**A**) Autoradiography image of segments of ruptured carotid plaque (left) and proximal healthy segments (right). Greater 18F-fluciclatide binding is visible within plaque rupture segments. Binding within the tissue segments (demarcated, black) was successfully blocked by the addition of a more concentrated un-labelled solution of fluciclatide (**B**). Areas showing the highest fluciclatide binding (demarcated, blue) exhibited a high degree of $\alpha_v\beta_3$ integrin expression (**C** and **D, arrow**) that also featured cellular staining for vascular endothelial cells (CD31, **E** and **F, arrow**) and inflammatory cells (CD68, **G** and **H, arrow**). Scale bar 1 mm in **C, E, G** and 75 µm in **D, F, H**.

Figure 2. Kinetic Analysis of Aortic 18F-Fluciclatide Uptake

Sagittal views of the thorax following kinetic analysis in two participants with (patient 1: **A-E**) and without (patient 2; **F-H**) aortic arch 18F-fluciclatide uptake. Computed tomography (CT) images confirm presence (**A**) or absence (**F**) of aortic arch calcification as a marker of established atheroma. Patlak slope (Ki) parametric images (**B** and **G**) identify focal uptake within the aortic arch in the region of atheroma (red arrow) localising to the vessel wall on the fused Patlak and CT images (**C** and **H**). Patlak modelling (**D**) confirms irreversible integrin binding within the region of aortic arch calcification (red arrow). Time activity curves (TAC) within the same region (**E**) show a persistently high blood pool fraction, but uptake within atheroma that exceeds the blood pool fraction beyond 40 min (dashed line).

1
2
3
4
5
6
7
8
9
10
11
12
13
14
15
16
17
18
19
20
21
22
23
24
25
26
27
28
29
30
31
32
33
34
35
36
37
38
39
40
41
42
43
44
45
46
47
48
49
50
51
52
53
54
55
56
57
58
59
60

Figure 3. 18F-Fluciclatide Aortic Uptake

Patient 3: Modified coronal view of the aortic arch showing radiotracer uptake at the inner curvature of the aortic arch related to a region of aortic calcification. This activity is demonstrated on axial sections of the aorta **(i and ii).** Red lines indicate the adventitial borders of the aortic arch used for quantification of PET uptake. **Patient 4:** Sagittal view of the thorax displaying focal 18F-fluciclatide uptake within a region of vascular calcification in the aortic arch.

Figure 4. 18F-Fluciclatide Uptake, Atheroma Burden and Clinical Stability

Graphs displaying the relationship between aortic 18F-fluciclatide uptake and aortic plaque burden, assessed using both the plaque volume **(A)** and calcium score **(B)**. Moreover 18F-Fluciclatide uptake was greater in patients with *unstable* (recent myocardial infarction) versus *stable* (no recent cardiovascular events) atherosclerotic disease **(C)**.
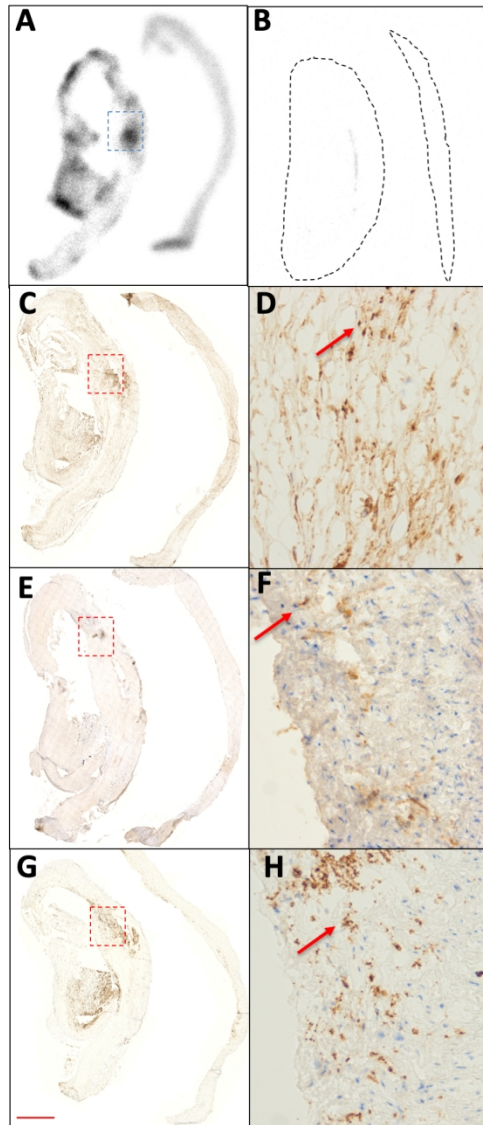
Figure 1. 18F-Fluciclatide Uptake in Carotid Atheroma

(A) Autoradiography image of segments of ruptured carotid plaque (left) and proximal healthy segments (right). Greater 18F-fluciclatide binding is visible within plaque rupture segments. Binding within the tissue segments (demarcated, black) was successfully blocked by the addition of a more concentrated un-labelled solution of fluciclatide (B). Areas showing the highest fluciclatide binding (demarcated, blue) exhibited a high degree of αvβ3 integrin expression (C and D, arrow) that also featured cellular staining for vascular endothelial cells (CD31, E and F, arrow) and inflammatory cells (CD68, G and H, arrow). Scale bar 1 mm in C, E, G and 75 μm in D, F, H.

190x253mm (225 x 225 DPI)
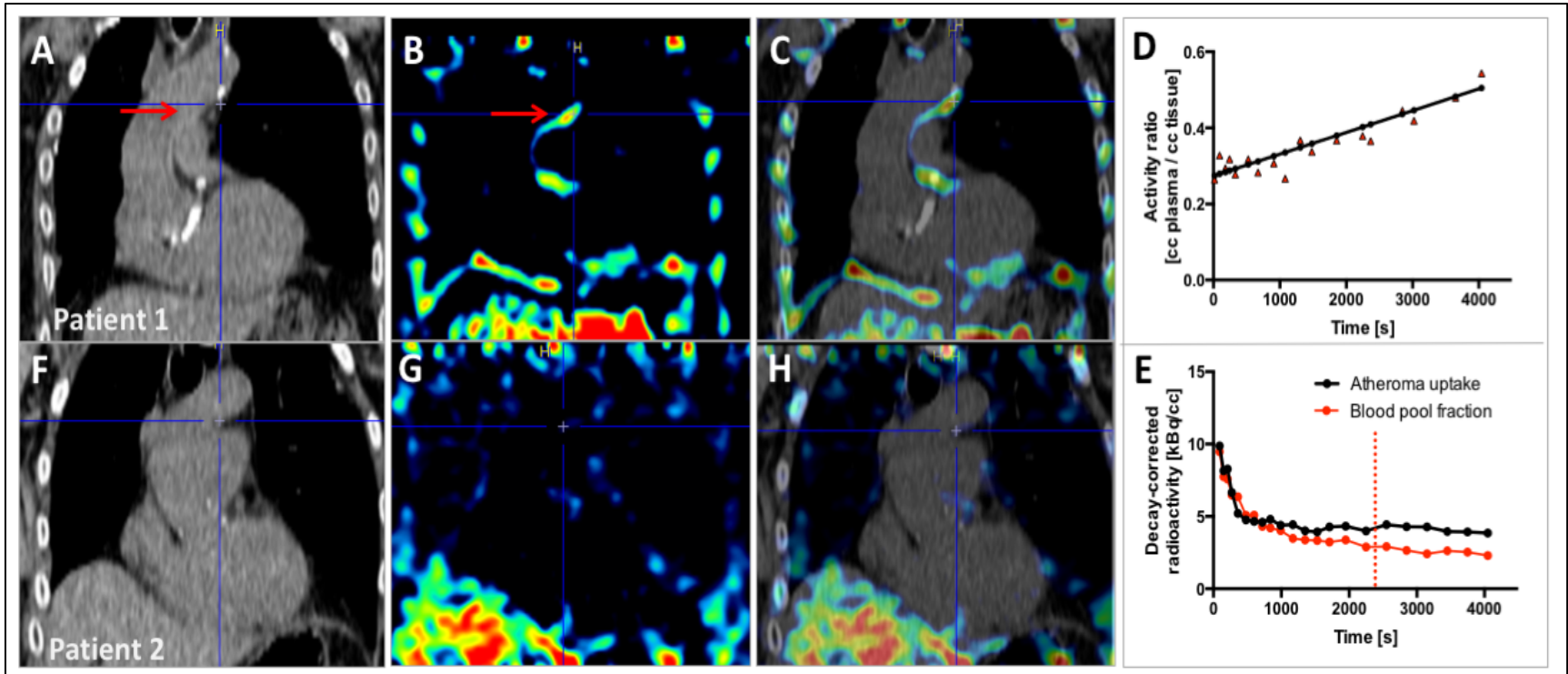
1
2
3
4
5
6
7
8
9
10
11
12
13
14
15
16
17
18
19
20
21
22
23
24
25
26
27
28
29
30
31
32
33
34
35
36
37
38
39
40
41
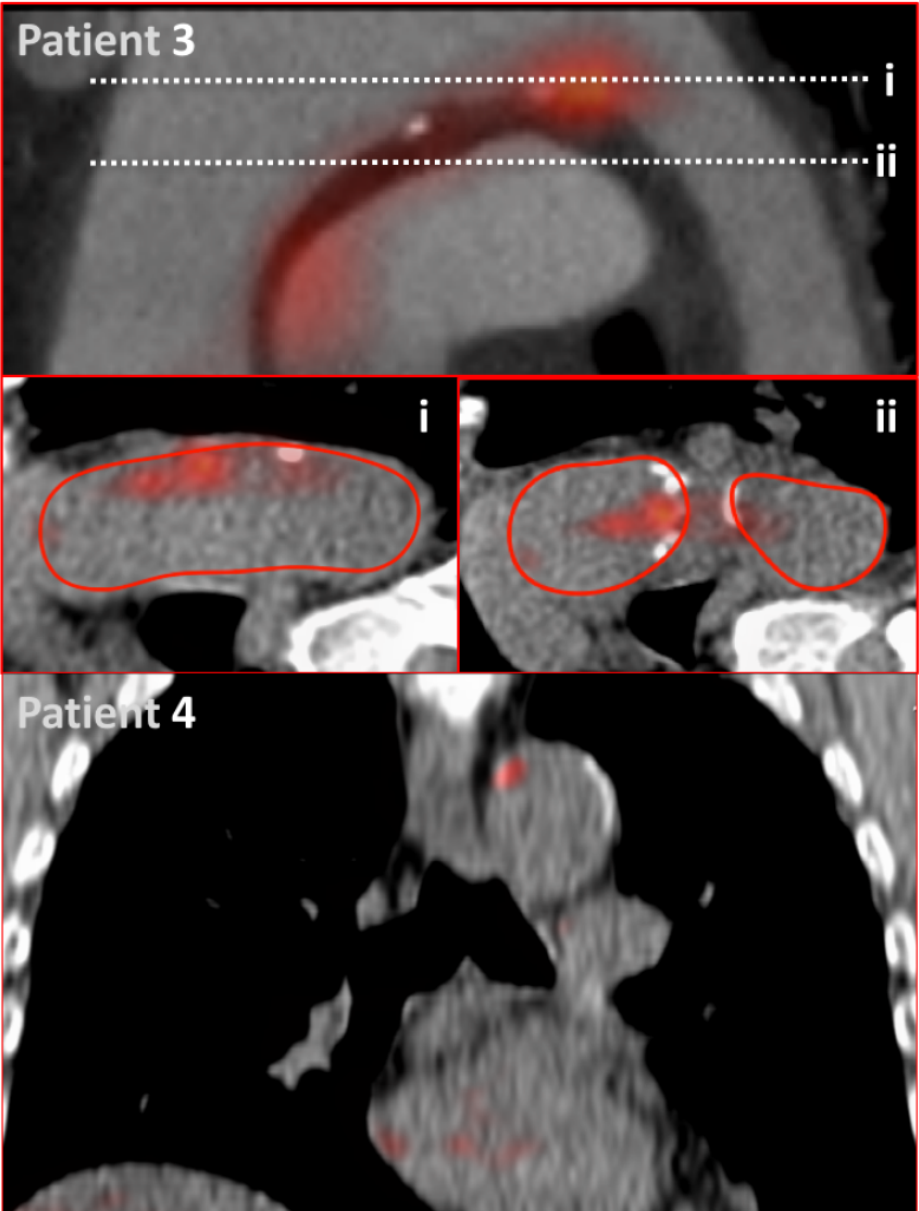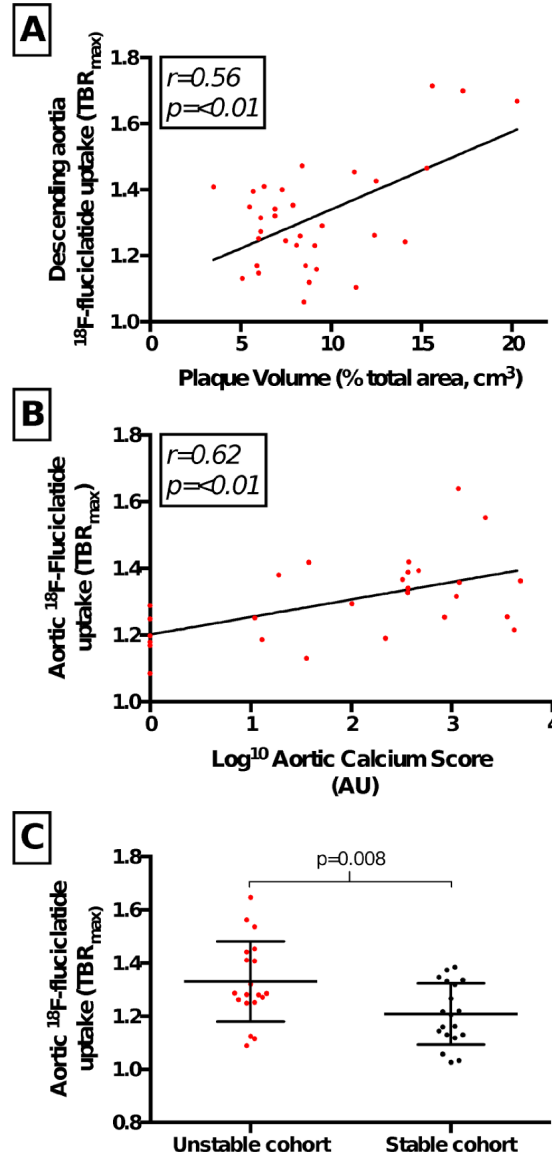
STROBE Statement—Checklist of items that should be included in reports of *cross-sectional studies*

	Item No	Recommendation	Page No
Title and abstract	1	(*a*) Indicate the study's design with a commonly used term in the title or the abstract	2
		(*b*) Provide in the abstract an informative and balanced summary of what was done and what was found	2
Introduction			
Background/rationale	2	Explain the scientific background and rationale for the investigation being reported	5
Objectives	3	State specific objectives, including any prespecified hypotheses	6
Methods			
Study design	4	Present key elements of study design early in the paper	7
Setting	5	Describe the setting, locations, and relevant dates, including periods of recruitment, exposure, follow-up, and data collection	7-9
Participants	6	(*a*) Give the eligibility criteria, and the sources and methods of selection of participants	7
Variables	7	Clearly define all outcomes, exposures, predictors, potential confounders, and effect modifiers. Give diagnostic criteria, if applicable	9-10
Data sources/ measurement	8*	For each variable of interest, give sources of data and details of methods of assessment (measurement). Describe comparability of assessment methods if there is more than one group	*9-10*
Bias	9	Describe any efforts to address potential sources of bias	11
Study size	10	Explain how the study size was arrived at	
Quantitative variables	11	Explain how quantitative variables were handled in the analyses. If applicable, describe which groupings were chosen and why	7-11
Statistical methods	12	(*a*) Describe all statistical methods, including those used to control for confounding	11
		(*b*) Describe any methods used to examine subgroups and interactions	11
		(*c*) Explain how missing data were addressed	
		(*d*) If applicable, describe analytical methods taking account of sampling strategy	11
		(*e*) Describe any sensitivity analyses	11
Results			
Participants	13*	(a) Report numbers of individuals at each stage of study—eg numbers potentially eligible, examined for eligibility, confirmed eligible, included in the study, completing follow-up, and analysed	12
		(b) Give reasons for non-participation at each stage	
		(c) Consider use of a flow diagram	
Descriptive data	14*	(a) Give characteristics of study participants (eg demographic, clinical, social) and information on exposures and potential confounders	25
		(b) Indicate number of participants with missing data for each variable of interest	
Outcome data	15*	Report numbers of outcome events or summary measures	
Main results	16	(*a*) Give unadjusted estimates and, if applicable, confounder-adjusted estimates and their precision (eg, 95% confidence interval). Make clear which confounders were adjusted for and why they were included	12-16

		(*b*) Report category boundaries when continuous variables were categorized	12-16
		(*c*) If relevant, consider translating estimates of relative risk into absolute risk for a meaningful time period	
Other analyses	17	Report other analyses done—eg analyses of subgroups and interactions, and sensitivity analyses	

Discussion

Key results	18	Summarise key results with reference to study objectives	17-20
Limitations	19	Discuss limitations of the study, taking into account sources of potential bias or imprecision. Discuss both direction and magnitude of any potential bias	17-20
Interpretation	20	Give a cautious overall interpretation of results considering objectives, limitations, multiplicity of analyses, results from similar studies, and other relevant evidence	17-20
Generalisability	21	Discuss the generalisability (external validity) of the study results	17-20

Other information

Funding	22	Give the source of funding and the role of the funders for the present study and, if applicable, for the original study on which the present article is based	21

*Give information separately for exposed and unexposed groups.

Note: An Explanation and Elaboration article discusses each checklist item and gives methodological background and published examples of transparent reporting. The STROBE checklist is best used in conjunction with this article (freely available on the Web sites of PLoS Medicine at http://www.plosmedicine.org/, Annals of Internal Medicine at http://www.annals.org/, and Epidemiology at http://www.epidem.com/). Information on the STROBE Initiative is available at www.strobe-statement.org.

Supplementary Text and Data

Computed Tomography Acquisition

Immediately after PET acquisition, thoracic CT angiography was performed: 330 ms rotation time, 100 (body mass index <25 kg/m^2) or 120 (body mass index >25 kg/m^2) kV tube voltage, 160-245 mAs tube current, 3.8 mm/rotation table feed, prospective (heart rate regular and <60 /min), or retrospective (heart rate >60 /min) electrocardiogram-gated. Depending on body mass index, a bolus of 80-100 mL contrast (400 mgI/mL; Iomeron, Bracco, Milan, Italy) was injected intravenously at 5 mL/s, after determining the appropriate trigger delay with a test bolus of 20 mL contrast material.

PET Imaging

Kinetic Analysis

PET data were reconstructed (Ultra-HD, 2 iterations, 21 subsets, 256 pixels, 1.6-mm pixel size) in a dynamic profile using the following time frames; 60s x 5, 120s x 5, 180s x 5, 300s x 8. Regions of interest (ROI's) were drawn both in the blood pool and sites of aortic atheroma visible on CT and used to derive time activity curves after decay correction. These were used to define a timeframe for static imaging based upon the point at which optimum contrast between blood pool and tissue activity was observed. To define 18F-fluciclatide uptake in aortic atheroma, a kinetic modeling input function calculation was based on the PET image-derived activity curve from the aortic blood pool.(8) (PMod version 4.3.1, Pmod technologies limited, Switzerland). This input function was applied to a tissue activity curve generated from ROI's placed in the myocardial interventricular septum, to estimate the tissue influx rate Ki (the slope

of the linear regression) and the volume of distribution (the intercept with the y axis) using a 2-

tissue irreversible Patlak model, with t* set to 20 min, as described previously (9,11). Thoracic

18F-fluciclatide dynamic activity was then normalized for the blood-pool input function on a

voxel-by-voxel basis, and after 3D Gaussian filtering (5-mm FWHM), a parametric 3-dimensional

image of 18F-fluciclatide uptake was generated accordingly. Using this image, regions of 18F-

fluciclatide binding in the vasculature were identified and manually delineated for subsequent

Ki analysis.

Histological Processing and Analysis

After obtaining informed consent, four human carotid intimal samples were obtained from

patients undergoing carotid endarterectomy for symptomatic carotid artery atherosclerotic

disease. Segments of dissected carotid atheroma were frozen in mounting medium. The tissue

samples were then cut in sequential, longitudinal 4 μm and 20 μm slices sections at -20°C and

thaw-mounted onto microscope slides. Effort was made to align segments of ruptured plaque

alongside non-atheromatous segments within the same slide. The slides were then dried for 15

min and spray-fixed with neutral buffered formalin. After rinsing in distilled water the 4 μm

sections were stained with hematoxylin-eosin (HE) and van-Gieson (VG) for conventional

histopathological examination. In order to optimize immunohistochemistry, an antigen-

unmasking step was performed by microwave treatment for 30 s. Endogenous peroxidase was

blocked by incubation with hydrogen peroxide for 5 min. Sections were subsequently incubated

with the primary antibodies; smooth muscle actin, CD31, CD68 (clone PG-M1), and integrin $\alpha_V\beta_3$

antibody, clone LM609 (Millipore) for 30 min at room temperature. After washing, the sections

were incubated with Envision Flex (DAKO, K5007) for 30 min at room temperature, followed by

incubation with diaminobenzamine (Sigma) for 10 min. The slides were finally counterstained

with hematoxylin and digitally imaged (Axioscan.Z1, Zeiss, UK).

Clinical PET systems have limited resolution. To gain more detailed information about the

precise localization of 18F-fluciclatide binding in atherosclerotic tissue, we undertook

autoradiography. The 20 µm frozen sections adjacent to those used for immunohistochemical

analysis were warmed to room-temperature and bathed in a solution of 18F-fluciclatide at a

concentration close to in vivo imaging concentrations (1 kBq/mL) for 60 minutes and then

rinsed with phosphate buffer solution. An unlabeled highly concentrated solution of fluciclatide

was added to selected slides in order to competitively bind to $\alpha_v\beta_3$ to assess for non-specific

tracer uptake. A freshly blanked phosphor screen was then placed over the slides and an

overnight exposure undertaken. The screen was read using a FujiFilm FLA-5100 Fluorescent

Image Analyser (Raytek Scientific Limited, Sheffield, UK). Sections were then manually

registered and examined for co-localization with histological markers of atherosclerotic disease

activity.

Table S1 – Reproducibility Analysis

18F-Fluciclatide Activity	Mean absolute difference[a]	Intra-class coefficient[b]
Superior Vena Cava		
Mean SUV *(SUV [kBq/cc])*	-0.11 (-0.36 – 0.15)	0.947
Aorta		
Mean SUV *(SUV [kBq/cc])*	-0.005 (-0.14 – 0.13)	0.986
Mean SUV$_{MDS}$ *(SUV [kBq/cc])*	0.01 (-0.17 – 0.15)	0.980
Max SUV *(SUV [kBq/cc])*	0.07 (-0.13 – 0.27)	0.971
Max SUV$_{MDS}$ *(SUV [kBq/cc])*	0.06 (-0.22 – 0.34)	0.957
Mean TBR	0.04 (-0.02 – 0.10)	0.954
Mean TBR$_{MDS}$	0.04 (-0.04 – 0.10)	0.940
Max TBR	0.08 (-0.01 – 0.16)	0.912
Max TBR$_{MDS}$	0.07 (-0.03 – 0.17)	0.919
SUV $_{Target-background}$	0.19 (-0.05 – 0.43)	0.612

[a] Mean difference between TBR$_{max}$ measurements (95% limits of agreement), and [b] ICC values for 18F-Fluciclatide throughout the thoracic aorta and SVC.

Abbreviations: ICC: intraclass correlation coefficient; MDS: most diseased segment; TBR: tissue to background ratio; SVC: Superior Vena Cava

Table S2 – Baseline demographic data

	All (n=46)	Stable Atherosclerosis (n=27)	Stable atherosclerosis; matched group (n=19)	Unstable Atherosclerosis (n=19)	P value
Age (years)	66±10	70±8	68±7	61±12	0.04
Male Sex	34 (74)	20 (74)	15 (79)	14 (74)	0.71
BMI (kg/m^2)	28±4	28±4	26±4	29±5	0.59
Systolic BP (mmHg)	140±22	149±19	151±18	127±19	<0.001
18F-Fluciclatide dose (MBq)	226±13	225±13	225±13	228±14	0.55
Cardiovascular History					
Angiographically documented CAD	26 (57)	7 (26)	1 (5)	19 (100)	<0.001
Prev MI	24 (52)	5 (19)	0 (0)	19 (100)	<0.001
Prev PCI	20 (43)	2 (7)	0 (0)	18 (95)	<0.001
Prev CVD	4 (11)	4 (14)	3 (16)	0 (0)	0.08
Risk Factors					
Current smoker	9 (20)	1 (4)	0 (0)	8 (42)	0.001
Diabetes Mellitus	6 (13)	4 (14)	2 (11)	2 (11)	0.99
Prior hypertension	23 (50)	18 (67)	11 (58)	6 (32)	0.11
Prior Hypercholesterolemia	25 (54)	12 (44)	6 (32)	12 (63)	0.03
hs-CRP (mg/l)	3.5 [1.4-7.8]	2.7 [1.4-5.8]	3.0±2.4	5.6 [2.0-11.7]	<0.001
Log$_{10}$ hs-CRP (mg/l)	0.51±0.51	0.41±0.44	0.48±0.38	0.65±0.56	<0.001
Medications					
Aspirin	28 (61)	10 (37)	5 (26)	19 (100)	<0.001
Clopidogrel	19 (41)	4 (14)	3 (16)	19 (100)	<0.001
Statin	31 (67)	13 (48)	5 (26)	19 (100)	<0.001
β-Blocker	27 (59)	8 (30)	2 (11)	19 (100)	<0.001
ACEi/ARB	31 (67)	10 (37)	4 (21)	18 (95)	<0.001
Calcium Channel Blocker	7 (15)	6 (22)	4 (21)	1 (5)	0.11

Categorical data are displayed as n (%). Normally distributed data displayed as mean±SD. Non-normally distributed data displayed as median [interquartile range].

IHD - ischemic heart disease; AS - aortic stenosis; CAD - coronary artery disease; MI - myocardial infarction; CVD – cerebrovascular disease; PCI - percutaneous coronary intervention; hs-CRP - high sensitivity c-reactive protein; ACEi - ACE-inhibitor; ARB - Angiotensin Receptor Blocker.

* P-values are quoted for comparisons between matched stable and unstable groups.

Table S3 – Imaging Results

	All (n=46)	Stable Atherosclerosis (n=27)	Matched Stable Atherosclerosis (n=19) [Ψ]	Unstable Atherosclerosis (n=19)	P value[*]
18F-Fluciclatide PET uptake					
SVC (SUV_{mean})	2.74±0.49	2.62±0.46	2.54±0.40	2.9±0.48	0.02
Whole aorta (mean SUV_{max})	3.59±0.62	3.40±0.62	3.19±0.65	3.84±0.55	0.001
Ascending aorta (mean SUV_{max})	3.60±0.66	3.42±0.70	3.16±0.56	3.87±0.51	<0.001
Aortic Arch (mean SUV_{max})	3.51±0.62	3.29±0.61	3.05±0.52	3.84±0.48	<0.001
Descending aorta (mean SUV_{max})	3.61±0.68	3.46±0.65	3.28±0.65	3.83±0.66	0.01
Whole aorta (mean TBR_{max})	1.32±0.14	1.30±0.12	1.26±0.09	1.33±0.18	0.14
Ascending aorta (mean TBR_{max})	1.32±0.16	1.31±0.17	1.25±0.10	1.34±0.17	0.05
Aortic Arch (mean TBR_{max})	1.30±0.14	1.26±0.14	1.21±0.1	1.33±0.15	0.008
Descending aorta (mean TBR_{max})	1.32±0.17	1.32±0.13	1.29±0.11	1.33±0.21	0.56
CT Calcium Score					
Whole aorta (AU)	95 [0-852]	326 (11-1114)	36 (0-469)	19 [0-483)	0.85
Ascending aorta (AU)	0 [0-11]	0 (0-46)	0 (0-0)	0 [0-0}	0.15
Aortic arch (AU)	29 [0-352]	102 (0-586)	13 (0-469)	0 [0-263]	0.76
Descending aorta (AU)	7.5 [0-78]	0 (0-123)	0 (0-123)	8 [0-71]	0.43
CTA Plaque analysis (descending aorta)					
Mean wall thickness (% vessel diameter)	10.3±4.9	8.4±2.8	8.4±3.1	14.0±6.3	0.003
Plaque burden (% total volume)	9.1±3.9	7.7±2.3	7.7±2.5	12.0±4.7	0.004

[Ψ] *Stable group subjects paired to equivalent calcium score in unstable group.*

1
2
3
4
5
6
7
8
9
10
11
12
13
14
15
16
17
18
19
20
21
22
23
24
25
26
27
28
29
30
31
32
33
34
35
36
37
38
39
40
41
42
43
44
45
46
47
48
49
50
51
52
53
54
55
56
57
58
59
60

[*]*P-values are quoted for comparisons between matched stable and unstable groups.*

SUV - standard uptake value; SVC – superior vena cava; TBR - tissue-to-background ratio